RSC Applied Polymers

ROYAL SOCIETY OF CHEMISTRY

PAPER

View Article Online
View Journal | View Issue

Cite this: *RSC Appl. Polym.*, 2024, **2**, 656

Triple click chemistry for crosslinking, stiffening, and annealing of gelatin-based microgels†

Chun-Yi Chang,[a] Han Nguyen,[a] Ellen Frahm,[b] Keith Kolaczyk [b] and Chien-Chi Lin *[a,b,c,d]

Received 15th November 2023,
Accepted 22nd March 2024

DOI: 10.1039/d3lp00249g

rsc.li/rscapplpolym

Microgels are spherical hydrogels with physicochemical properties ideal for many biomedical applications. For example, microgels can be used as individual carriers for suspension cell culture or jammed/annealed into granular hydrogels with micron-scale pores highly permissive to molecular transport and cell proliferation/migration. Conventionally, laborious optimization processes are often needed to create microgels with different moduli, sizes, and compositions. This work presents a new microgel and granular hydrogel preparation workflow using gelatin-norbornene-carbohydrazide (GelNB-CH). As a gelatin-derived macromer, GelNB-CH presents cell adhesive and degradable motifs while being amenable to three orthogonal click chemistries, namely the thiol-norbornene photo-click reaction, hydrazone bonding, and the inverse electron demand Diels–Alder (iEDDA) click reaction. The thiol-norbornene photo-click reaction (with thiol-bearing crosslinkers) and hydrazone bonding (with aldehyde-bearing crosslinkers) were used to crosslink the microgels and to realize on-demand microgel stiffening, respectively. The tetrazine-norbornene iEDDA click reaction (with tetrazine-bearing crosslinkers) was used to anneal microgels into granular hydrogels. In addition to materials development, we demonstrated the value of the triple-click chemistry granular hydrogels *via* culturing human mesenchymal stem cells and pancreatic cancer cells.

1. Introduction

Microgels are spherical hydrogels with physicochemical properties ideal for many biomedical applications. Microgels can be used as individual carriers for suspension cell culture or be assembled into granular hydrogels through physical jamming or chemical annealing. Conventionally, microgels are manufactured using microfluidic systems, water-in-oil emulsions, or fragmentation of bulk gels.[1] In contrast to the nanometer-scale mesh sizes of chemically crosslinked hydrogels, granular hydrogels possess micron-scale pores that are highly permissive to molecular transport and less restrictive to cell proliferation and migration. As such, granular hydrogels are increasingly used in biomedical applications, particularly in promoting tissue regeneration. The Segura group pioneered in developing chemically annealed, granular hydrogels (macroporous annealing particles or MAP hydrogels) to facilitate wound healing and tissue regeneration.[2] For example, poly(ethylene glycol) (PEG) based microgels were crosslinked through a thiol-vinylsulfone reaction in a microfluidic chamber. The PEG-based microgels were then annealed through a transglutaminase-assisted amide bond formation between peptide crosslinkers containing lysine (K) and glutamine (Q) residues.

The physicochemical properties of granular hydrogels are collectively influenced by the properties of the microgels and the jamming/annealing processes. To fabricate microgels with different properties (*e.g.*, size, stiffness, bioactivity, *etc.*), one needs to alter the macromer compositions and fabrication/crosslinking processes. The jamming conditions or annealing chemistry further impacts the properties and stability of the granular hydrogels. Altogether, these properties dictate the behaviors of cells embedded within the granular hydrogels. For example, Qazi *et al.* showed that in hyaluronic acid (HA)-based granular gels, the microgel size, packing density, and the use of a matrix metalloproteinase (MMP)-degradable crosslinker controlled the cell sprouting length, tortuosity, and density.[1] Similarly, Liu *et al.* fabricated HA-based microgels with different sizes for annealing into a MAP hydrogel with various void fractions. They discovered that the void fraction affected the macrophage motility on the microgel surface

[a]*Weldon School of Biomedical Engineering, Purdue University, West Lafayette, IN 47907, USA. E-mail: lincc@iupui.edu*
[b]*Department of Biomedical Engineering, Indiana University-Purdue University Indianapolis, Indianapolis, IN 46202, USA*
[c]*Indiana University Melvin and Bren Simon Comprehensive Cancer Center, Indianapolis, IN 46202, USA*
[d]*Integrated Nanosystems Development Institute, Indianapolis, IN 46202, USA*
† Electronic supplementary information (ESI) available. See DOI: https://doi.org/10.1039/d3lp00249g

(*i.e.*, in the void space).[3] The authors also showed that higher stiffness of MAP gels enhanced cell growth.[4]

The current methods for fabricating microgels with different properties can be laborious.[5] For example, a standard microfluidic setup only allows for the preparation of microgels with one defined set of properties, such as stiffness. To fabricate microgels with a different degree of crosslinking, one must go through the fabrication and separation/cleaning process with a different set of macromer solutions (Fig. 1A), which can be time- and material-consuming. Alternatively, special high-throughput microfluidic devices may be used to accelerate the production of the microgels, but the microgels would still possess the same characteristics.[6] We sought to simplify/expedite the fabrication of microgels with different cross-linking degrees by using a post-gelation dynamic stiffening technique. Here, 'dynamic stiffening' refers to user-initiated secondary matrix stiffening at any given time post-gelation. The processes start with fabricating a large quantity of microgels either with a microfluidic droplet generator or inverse suspension (*i.e.*, oil-in-water emulsion) polymerization. Of note is that the crosslinked microgels should possess the ability to undergo secondary chemical reactions, such as on-demand stiffening. These microgels are then split into smaller groups, with each group differentially stiffened by adjusting the concentration of the stiffening reagent (Fig. 1B). As a result, microgels with different stiffness were readily prepared without repeating the labor-intensive fabrication and separation processes.

We leveraged our previously developed gelatin-norbornene-carbohydrazide (GelNB-CH) to fabricate microgels that can be dynamically stiffened.[7] As a gelatin-derivative, GelNB-CH is inherently bioactive (*i.e.*, gelatin is derived from collagen and contains peptide sequences for cell adhesion and MMP-mediated degradation) and amenable to three orthogonal click chemistries, namely the thiol-norbornene photo-click reaction (with thiol-bearing crosslinkers), hydrazone bonding (with aldehyde-bearing crosslinkers), and the inverse electron demand Diels–Alder (iEDDA) click reaction (with tetrazine-bearing crosslinkers). The thiol-norbornene photo-click reaction (Fig. 1C) and hydrazone bonding (Fig. 1D) are used to photo-crosslink the microgels and afford on-demand stiffening of microgels post-fabrication, respectively.[7] While previous work has demonstrated on-demand stiffening of GelNB-CH hydrogels using oxidized dextran (oDex) or oxidized HA (oHA), this bioactive macromer has not been used to fabricate microgels with dynamically tunable properties. Of note is that the crosslinking of GelNB-CH based microgels is performed with an off-stoichiometry ratio of thiol and norbornene moieties, intentionally leaving excess norbornene groups for annealing the microgels into MAP gels through the tetrazine-norbornene

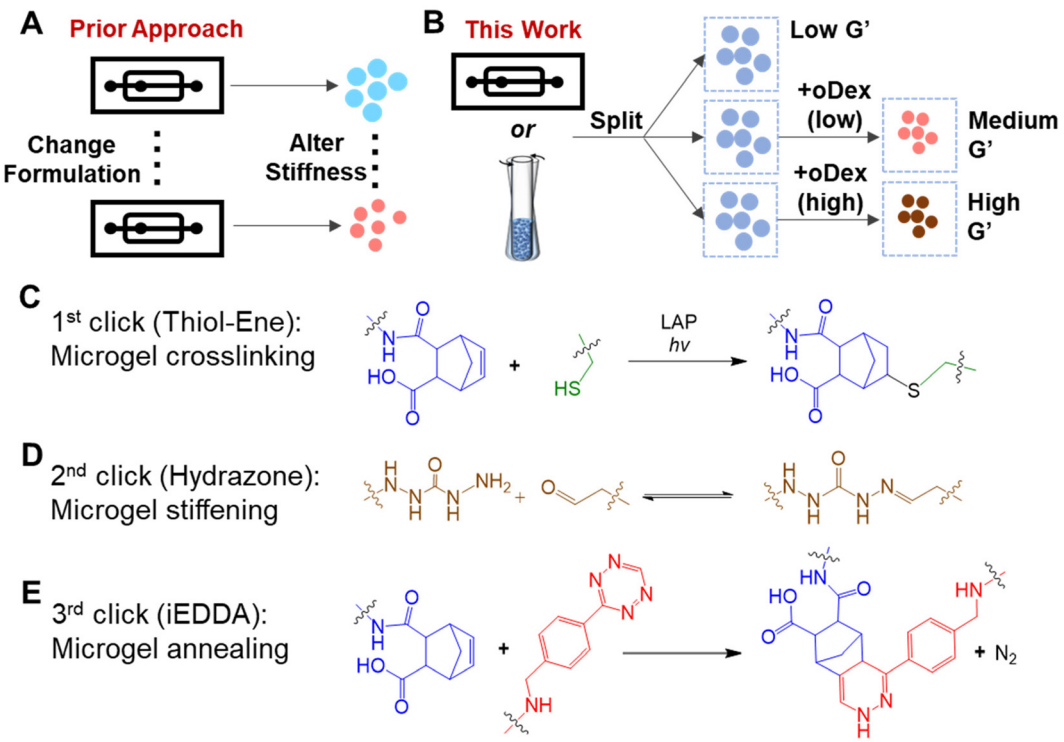

Fig. 1 Workflow of microgel synthesis and dynamic stiffening. (A) Prior approach for fabricating microgels with different stiffness. (B) Current study to efficiently generate microgels with different stiffness *via* post-fabrication dynamic stiffening. A large group of microgels were manufactured first, followed by dynamic differential stiffening using various concentrations of the stiffening reagent (*e.g.*, oxidized dextran, oDex). (C) Thiol-norbornene photo-click reaction for primary hydrogel crosslinking. (D) Hydrazone bonding for secondary stiffening of microgels. (E) iEDDA click reaction for annealing microgels of varying stiffness into TC-MAP scaffolds.

iEDDA click reaction (Fig. 1E).[4,8] Previous reports have shown that MAP gels could be prepared by combining thiol-norbornene photo-click chemistry and the norbornene-tetrazine iEDDA click reaction.[4,8] To the best of our knowledge, however, no prior work has integrated hydrazone bonding into thiol/tetrazine-norbornene click chemistry for MAP gel fabrication. Here, we developed triple-click chemistry MAP (TC-MAP) hydrogels and used them to culture human mesenchymal stem cells (hMSCs), pancreatic cancer cells, and cancer-associated fibroblasts (CAFs).

2. Materials and methods

2.1. Materials

Type B gelatin (225 Bloom) was purchased from Electron Microscopy Sciences. 8-Arm PEG (20 kDa) was purchased from JenKem Technology USA. 4-Arm PEG-thiol (PEG4SH, 10 kDa) and 4-arm PEG-amido succinic acid (PEG4ASA, 10 kDa) were acquired from Laysan Bio. Lithium phenyl-2,4,6-trimethylbenzoylphosphinate (LAP) and dextran (15–25 kDa) were purchased from Sigma-Aldrich. Sodium metaperiodate was purchased from Fisher Scientific. Tetrazine amine was purchased from Click Chemistry Tools. Carbic anhydride, carbohydrazide, and *N*-(3-dimethylaminopropyl)-*N*′-ethylcarbodiimide (EDC) hydrochloride were purchased from Acros Organics. HOBt hydrate was purchased from Oakwood Chemical. O-(7-Azabenzotriazole-1-yl)-*N,N,N,N*′-tetramethyluronium hexafluorophosphate (HATU) was purchased from Chem-Implex International. 5 wt% Pico-Surf in Novec 7500 was purchased from Sphere Fluidics. The Novec 7500 solution was purchased from 3M. PDMS (DOWSIL™ SE 1700) was purchased from Dow Chemical. HyClone Dulbecco's Modified Eagle's medium (DMEM, SH30243.01) and 100× antibiotic–antimycotic solution (SV30079.01) were acquired from Cytiva. Human fibroblast growth factor basic (bFGF) was purchased from Peprotech. Dulbecco's phosphate-buffered saline (DPBS) and fetal bovine serum (FBS, USDA Approved Origins) were purchased from Corning. 0.5% trypsin-EDTA was purchased from ThermoFisher (15400-054). FITC-dextran (2 MDa) was purchased from Millipore Sigma. Fibronectin/FN1 (E5H6X, 1 : 200 dilution) rabbit mAb (#26836), COL1A1 (E3E1X, 1 : 100 dilution) mouse mAb (#66948), and Alexa Fluor 555 anti-mouse IgG (H + L) (1 : 500 dilution, #4409S) were purchased from Cell Signaling. Donkey anti-rabbit IgG (H + L) (1 : 500 dilution) was purchased from Biotium (#20015). Rhodamine phalloidin (#PHDR1) was purchased from Cytoskeleton, Inc. DAPI (#AS-83210) was purchased from AnaSpec.

2.2. Macromer synthesis and characterization

GelNB-CH was synthesized using the method described in our previous study.[7] Briefly, gelatin was first modified with norbornene moieties by reacting primary amines of gelatin with carbic anhydride.[9] GelNB was purified by dialysis and collected from freeze-drying, followed by a secondary reaction with carbohydrazide through standard EDC/NHS-assisted carbodiimide chemistry. 8-Arm poly(ethylene glycol)-norbornene (PEG8NB) was synthesized based on a method reported by others.[10] The norbornene on PEG8NB was quantified to be ~82% (3.8 mM per wt% PEG8NB). Oxidized dextran (oDex) was prepared through the well-known sodium periodate-mediated oxidation.[11] Briefly, periodate ions attack the hydroxyl groups on C2, C3, and C4 on dextran, resulting in the ring opening of dextran and two aldehydes on the opened rings.[12] 4-Arm PEG-tetrazine (PEG4Tz) was synthesized by HATU-catalyzed conjugation of tetrazine amine to PEG4ASA. All macromer products were purified by dialysis against water for three days. The norbornene contents on GelNB were indirectly quantified using a fluoraldehyde assay that measured the amine concentration on modified gelatin. First, the total primary amine concentrations on pristine gelatin and GelNB-CH were determined using the fluoraldehyde reagent following the manufacturer's instructions without modification. The difference in amine concentration was calculated and used to represent the norbornene content. The content of carbohydrazide on GelNB-CH was quantified with TNBSA assay following the manufacturer's instructions without modification. The increases in the reading were calculated and used to represent the carbohydrazide content. Both norbornene and carbohydrazide modifications were also verified by nuclear magnetic resonance (NMR), as reported previously.[7]

2.3. Fabrication, stiffening, and annealing of GelNB-CH-based hydrogels

GelNB-CH bulk gels were fabricated through thiol-norbornene photopolymerization. A precursor solution consisting of 5 wt% GelNB-CH, 1 wt% PEG4SH, and 2 mM LAP was prepared and deposited in between glass slides that were separated by 1 mm thick spacers, followed by exposure to 365 nm UV light at 5 mW cm^{-2} for 2 min. The gels were transferred to a well plate containing PBS. After 1 hour, the swollen hydrogels were transferred to wells containing various concentrations of oDex (*i.e.*, 0.01/0.05/0.1 wt%) for 24 hours. The mechanical properties of the bulk gels were characterized using strain-sweep rheometry at a frequency of 1 Hz. Hydrogel sizes were measured by outlining the edge of the round bulk gels stiffened by different oDex contents, followed by calculating the surface areas of the round gels with ImageJ. The reduction in gel surface area were calculated by comparing the stiffened and non-stiffened gels.

GelNB-CH microgels were fabricated using either a microfluidic droplet generator or a water-in-oil emulsion method. Aqueous gel precursor solution was prepared using the same formulation as the bulk gel. Microdroplets were formed by flowing the water phase (precursor solution) and oil phase (2 wt% Pico-Surf in Novec 7500 solution) into a droplet generator prepared in-house.[13] By adjusting the flow rate of the water and oil phases (5 and 30 μL min^{-1}, respectively), the aqueous stream was "pinched" off by the oil phase into microdroplets, which were polymerized into microgels by

shining 365 nm UV light (5 mW cm^{-2}) on the microdroplets for 2 min.

For the microgels prepared from inverse suspension polymerization, 1 wt% of PEG8NB was supplemented to strengthen the cell-laden gelatin-based hydrogel against proteolytic degradation. 0.5 mL of the precursor solution was added to a 5 mL test tube filled with 0.5 mL of Novec 7500 solution containing 2 wt% Pico-Surf. The mixture was then subject to ~5 s of vortexing to generate microdroplets. The test tube, along with the microdroplets, was then exposed to UV light (4.5 mW cm^{-2}) for 2 minutes before the droplets merged back together. The GelNB-CH microgels formed after the UV exposure were washed thoroughly with PBS and collected through centrifugation. Microgels were separated into multiple microcentrifuge tubes for different degrees of stiffening with oDex (*i.e.*, 0, 0.01, 0.05, 0.1 wt%). After stiffening overnight, some microgels were taken out from the tubes for imaging and characterization of sizes by ImageJ.

MAP gels were fabricated with microgels prepared by inverse suspension polymerization. This is achieved by first washing the microgels with PBS in microcentrifuge tubes by centrifugation. After the microgels were washed thoroughly, they were resuspended in 0.5 wt% PEG4Tz/PBS solution and packed again by centrifugation. The supernatant was removed from the tubes, and the microgels were transferred to PDMS molds 3D-printed using a BIO X 3D printer (CELLINK). A few drops of the supernatant were added to the microgels, and the microgels were allowed to be annealed for 1 hour.

2.4. Characterization of GelNB-CH-based hydrogels

The size of the bulk gels before and after stiffening was tracked by taking pictures of the gels and measuring the size by outlining the area of the gels using ImageJ (scale set using the graduation on the ruler). The size change measured is the difference in percentage between the measured area of bulk gels before and after stiffening/incubation. The storage moduli of the bulk gels (45 μL) and the MAP gels (200 μL) were measured with an MCR 102 rheometer (Anton Paar) using strain-sweep rheometry. The strain values ranged from 0.1 to 5% at a constant 1 Hz frequency. The normal force applied to the gels during the measurements was 0.25 N for bulk gels and 0.1 N for MAP gels using an 8 mm plate. The storage moduli of the gels in the linear viscoelasticity range were averaged to obtain the G' value. The microgel size was tracked by imaging with a Lionheart FX microscope and measured with ImageJ. The MAP gels were tested for porosity (or void fraction) and stiffness. Frequency sweep rheometry, ranging from 0.1 to 100 rad s^{-1} at 1% strain, was performed to confirm the effective stiffness measurement within the linear viscoelastic range. To visualize and quantify the void fraction of the MAP gels, the gels were annealed in a 3D-printed cylindrical mold on a coverslip and perfused with 5 mg mL^{-1} FITC-dextran solution for 0.5 hours. Images of the MAP gels were taken with an Olympus FV1000 confocal microscope at 10× objective magnification. Three images of different areas of interest were taken for each MAP gel, and the thickness of each image is 200 μm (41 layers). Imaris software was used to reconstruct the stacked images, and ImageJ was used to quantify the void fraction. The quantification was done according to the method described by Qazi *et al.*[1] Briefly, the image files, after being imported to ImageJ, were adjusted to binary color using Huang's thresholding method. All the void space in each slice was outlined and selected, and the area was divided by the total area of a slice of the image to obtain a void fraction. Every image stack was measured for 21 layers (one every 10 μm). The results were averaged for each image stack, and the results from multiple image stacks were averaged again to obtain the mean of each MAP gel, which, in turn, was used to plot the mean and standard error of the mean.

2.5. hMSC culture and seeding on microgels

hMSCs were isolated from de-identified donor bone marrow (Lonza), cultured in low glucose DMEM supplemented with 10% FBS, 1% antibiotic/antimycotic, and 2 ng mL^{-1} bFGF and were used before passage 5. hMSCs were seeded on the microgel surface by combining the cell suspension with the microgels at a desired ratio (*e.g.*, 50 000 cells per 150 μL of microgels) in a centrifuge tube.[14,15] Then, the cell–microgel mixture was centrifuged at 1000 rpm for 3 minutes, and cells were allowed to settle on the microgels for 3 hours. Cell attachment on microgels was confirmed under a microscope before removing the supernatant. Cell-laden microgels were transferred from centrifuge tubes to a 24-well plate containing 2 mL of media and cultured for ~5 days at 37 °C with 5% CO_2.

Immunofluorescence staining of collagen and fibronectin was conducted on hMSC-seeded microgels. Cell-seeded microgels were fixed with 4% paraformaldehyde for 1 h at room temperature, washed with 0.3% Triton-X 3 times (10 minutes for each wash), and blocked with 0.3% Triton-X and 1% BSA solution overnight. The next day, samples were incubated overnight with primary antibodies–anti-COL1A1 mouse mAb (1 : 100) and anti-FN1 rabbit mAb (1 : 200). The following days, microgels were washed three times in wash buffer containing 0.3% Triton-X and 1% BSA (10 minutes for each wash) and then incubated with secondary antibodies AlexaFluor 555 for COL1A1 and AlexaFluor 488 for FN1 (1 : 500) for 2 hours. Rhodamine phalloidin was used after sample fixing and permeabilization for F-actin staining. Finally, the samples were washed with PBS 3 times, 10 minutes each, and counterstained for cell nuclei with DAPI for 1 hour.

2.6. Cancer cell spheroid assembly and encapsulation in TC-MAP gels

TdTomato-expressing Pa03C cells and green-fluorescent protein (GFP)-expressing CAF cells were cultured in high glucose DMEM supplemented with 10% FBS and 1% antibiotics/antimycotics on tissue culture plastics at 37 °C with 5% CO_2. The spheroids were assembled in Aggrewell according to the manufacturer's instructions with some modifications. Briefly, CAF (passage number < 40) and Pa03C cells (passage number < 20) were trypsinized from the culture plate, counted,

and added to a 24-well Aggrewell plate at a ratio of 5 CAF to 1 Pa03C. Each well contained 2×10^5 CAFs, 4×10^4 Pa03Cs, and 1 mL culture medium. The cells were mixed by pipetting. About 1200 spheroids were obtained two days after seeding the cells.

To create soft and stiff TC-MAP gels, we 3D-printed two concentric rectangular PDMS wells (Fig. S1†). The inner rectangle was a mold for depositing microgels, whereas the outer was for the cell culture medium. Microgels were prepared according to the method described in 2.3, except that everything was sterile. Microcentrifuge tubes, test tubes, and molds were autoclaved, and the rest were used as purchased. 0.01 and 0.1 wt% oDex were used for stiffening the microgels for soft and stiff TC-MAP gels, respectively. Cell spheroids prepared using the abovementioned method were harvested by centrifugation. After the culture medium was removed, cell spheroids were added to the microgel suspension supplemented with 0.5 wt% PEG4Tz for microgel annealing. The mixtures were centrifuged at 6000 rpm for 1 minute to remove excess liquid. The sediment was gently transferred to the printed PDMS mold, and the surface of the constructs was gently smoothened with a cell scraper. The constructs were allowed to anneal for 1 hour at 37 °C, followed by addition of a fresh culture medium. The constructs were cultured at 37 °C with 5% CO_2. The cell morphology of these constructs was imaged over time with a BC43 confocal microscope (Oxford Instruments).

2.7. Statistics

All numerical data analyses and statistical analyses were performed using GraphPad Prism software. All numerical data presented have been tested for normality and variance homogeneity, using the Shapiro–Wilk test and Brown–Forsythe test, respectively. One-way ANOVA was performed to analyze the stiffness and size of bulk GelNB-CH hydrogels (Fig. 2C, 2E) and stiffness of MAP gels (Fig. S4†). Single, double, triple, and quadruple asterisks represent $p < 0.05$, 0.01, 0.001, and 0.0001, respectively. Tukey's multiple comparison test was used for *post-hoc* analyses for ANOVA. The size of the microgels, either the data from one single batch or 3 batches (Fig. 3B, 5B, Fig. S3A and S3B†), and void fraction of MAP gels (Fig. 6C) did not pass the normality test, and a non-parametric test was performed on the data, followed by Dunn's multiple comparison test for significant difference. All microgel size measurements were collected from 3 biological repeats, with each repeat including more than 50 microgels (*i.e.*, technical repeats) for each group. Similarly, 3 MAP gels (*i.e.*, biological repeats) were

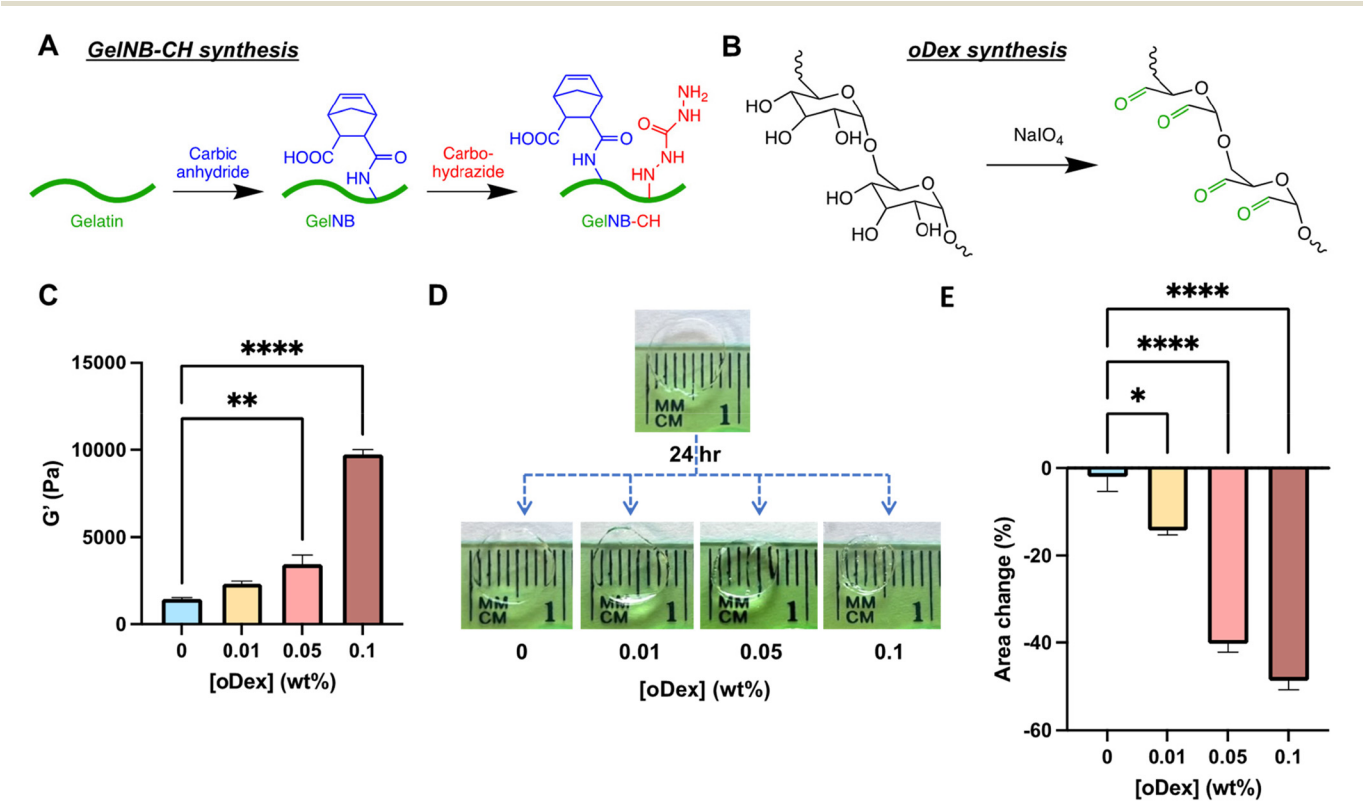

Fig. 2 Synthesis of GelNB-CH and oDex and characterization of dynamically stiffened hydrogels. (A) Schematic of GelNB-CH synthesis. (B) Schematic of oDex synthesis. (C) Effect of oDex concentration on the stiffening of bulk GelNB-CH (5 wt%) hydrogels crosslinked by PEG4SH (1 wt%). Hydrogels were incubated in oDex solution overnight at room temperature. (D) Photographs of bulk GelNB-CH hydrogels stiffened with different oDex concentrations. (E) Area change of GelNB-CH bulk gels after incubation in PBS or oDex (0.01/0.05/0.1 wt%) for 24 h. $N = 3$ for each group, data presented are mean ± SEM, and *: $p < 0.05$, **: $p < 0.01$, and ****: $p < 0.0001$. The statistical analyses in (C) and (E) are comparisons between individual stiffened groups and control (0 wt% oDex).

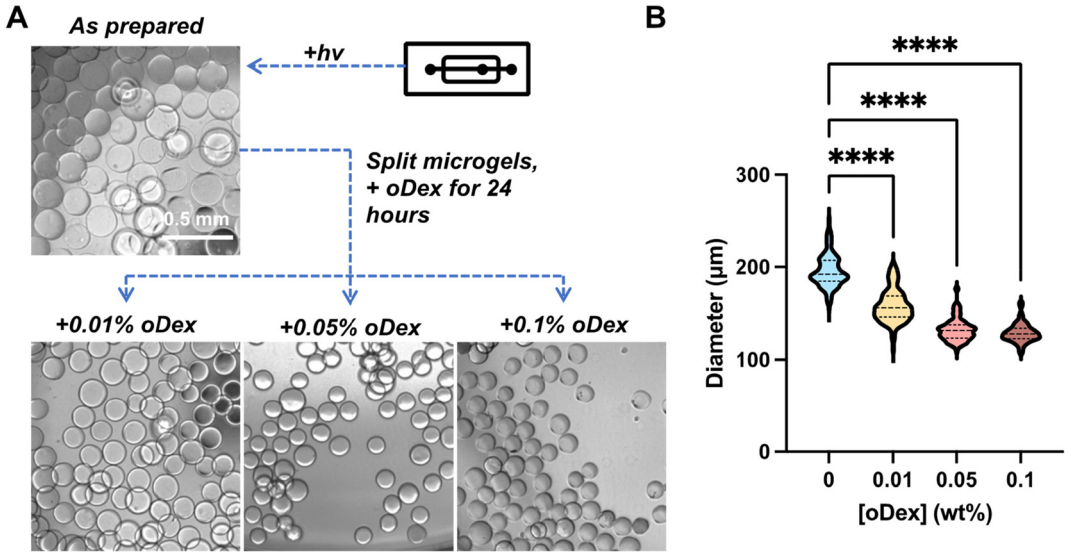

Fig. 3 Fabrication of GelNB-CH microgels *via* a microfluidic droplet generator. (A) Representative images of non-stiffened (as prepared) GelNB-CH microgels using a microfluidic droplet generator and microgels stiffened with different oDex concentrations (scale: 0.5 mm). (B) Size quantification of non-stiffened and oDex-stiffened microgels using the microgels fabricated with a microfluidic droplet generator. 0 wt%: n = 227, 0.01 wt%: n = 114, 0.02 wt%: n = 115, and 0.05 wt%: n = 86. ****: $p < 0.0001$. The statistical analyses in (B) are comparison between individual stiffened groups and control (0 wt% oDex).

measured for void fraction, and for each MAP gel, 3 regions of interest (*i.e.*, biological repeats) were selected for measuring the averaged void fraction. Statistical comparison was made between stiffened groups and the non-stiffened controls.

3. Results and discussion

3.1. Synthesis, crosslinking, characterization, and dynamic stiffening of GelNB-CH hydrogels

We previously showed that gelatin could be sequentially modified with carbic anhydride and carbohydrazide, yielding GelNB-CH, a bioactive macromer dually modified with norbornene and carbohydrazide for orthogonal crosslinking and dynamic stiffening (Fig. 2A).[7] Successful modification of norbornene and carbohydrazide moieties on gelatin was verified by proton NMR (Fig. S2A†) and quantified *via* fluoraldehyde and TNBSA assays. The total primary amine concentrations on pristine gelatin and GelNB-CH were quantified to be 3.76 and 1.07 mM per wt% of macromer, respectively (Fig. S2B†). Hence, the NB content on GelNB-CH was estimated to be 2.7 mM per wt% macromer. The total carbohydrazide concentrations on GelNB-CH were estimated to be 3.5 mM per wt% of GelNB-CH (Fig. S2C†). The primary crosslinking of GelNB-CH was achieved by photopolymerization with multifunctional thiol crosslinkers (*e.g.*, PEG4SH, Fig. 1B), whereas the secondary stiffening was achieved by diffusing oDex into the hydrogels. The aldehyde groups on oDex (Fig. 2B) readily reacted with the pendant CH moieties on GelNB-CH *via* hydrazone bonding (Fig. 1C), resulting in dynamic stiffening of the hydrogels.

We first evaluated the effect of hydrazone-mediated stiffening by incubating the hydrogels in PBS containing 0 to 0.1 wt% oDex overnight, followed by measuring the shear moduli of the bulk hydrogel with strain-sweep rheometry. As shown in Fig. 2C, the storage moduli of the hydrogels increased markedly at higher oDex concentrations. Specifically, the GelNB-CH/PEG4SH hydrogels were crosslinked to $G' \approx 1.8$ kPa pre-stiffening. After overnight oDex incubation, the moduli went up drastically to ~10 kPa. This range of stiffening was relevant to many healthy and diseased tissues, including pancreatic cancer stroma.[16,17] In addition to increases in gel stiffness, significant shrinkage of the hydrogels was noted after oDex incubation (Fig. 2D). Qualitatively, incubating the hydrogels in 0.01 wt% to 0.1 wt% of oDex solution led to ~5% to ~30% shrinkage in diameters of the bulk circular hydrogel discs, which were equivalent to ~16% to ~50% changes in areas (Fig. 2E). The sharp increases in hydrogel storage moduli and significant decreases in gel size were indicative of additional hydrazone bond formation between the hydrazide groups on GelNB-CH and the aldehyde moieties on the infiltrating oDex.

3.2. Microfluidic fabrication of GelNB-CH microgels and dynamic crosslinking *via* secondary hydrazone bonding

In traditional microgel fabrication methods (*e.g.*, microfluidic devices), one set of operating parameters can only produce a batch of microgels with similar properties regardless of the throughput (Fig. 1A).[6] Fabrication of microgels with different stiffness can be a laborious process, considering the various operating parameters involved (*e.g.*, the size of the channels, flow rates and ratios of aqueous and oil phases, *etc.*). In this

work, we sought to demonstrate that microgels of various storage moduli can be prepared from one batch of microgels with post-fabrication hydrazone-mediated stiffening (Fig. 1B and 2C). We set up a microfluidic droplet generator upstream of a light source (365 nm) for initiating the thiol-norbornene photopolymerization. GelNB-CH, PEG4SH, and photoinitiator LAP were pre-mixed at desired concentrations and flowed through the microfluidic droplet generator. The droplets were generated in the device, run through the tubing, and exposed to 365 nm light irradiation for photopolymerization of GelNB-CH/PEG4SH microgels. As prepared, the diameters of these microgels were approximately 195.7 ± 1.2 μm (mean ± SEM) (Fig. 3A and B). These microgels were collected, washed, split into several fractions, and treated with oDex at different concentrations (Fig. 3A). The diameters of the oDex-treated microgels were 158.1 ± 1.7 μm, 132.2 ± 1.1 μm, and 128.8 ± 1.1 μm (mean ± SEM) for 0.01 wt%, 0.05 wt%, and 0.1 wt% oDex, respectively. Similar to that observed in the bulk gel stiffening (Fig. 2C–E), incubating microgels with oDex led to significant shrinkage of the microgels (Fig. 3A) and all oDex-treated microgels remained narrow in size distribution (Fig. 3B). The trend was also observed in the averaged result of 3 biological repeats (Fig. S3A†), in which the size of non-stiffened microgels decreased from 226.2 ± 30 μm to 198.6 ± 39 μm, 164.3 ± 34.9 μm, and 150.7 ± 31.3 μm (mean ± SEM), using 0.01, 0.05, and 0.1 wt% oDex, respectively.

While the reduction of microgel sizes post-oDex incubation was indicative of additional hydrazone crosslinking and stiffening in the GelNB-CH microgels, there was some discrepancy in the degree of bulk gel stiffening (Fig. 2C) and hydrogel size reduction (Fig. 2E and 3B). Specifically, there was about a 300% increase in bulk gel moduli between 0.05 wt% and 0.1 wt% oDex treatment but the size changes were only around 10%. It is worth noting that the microgels and bulk gels were prepared from gelatin and PEG derivatives and the stiffening was performed using oxidized dextran. As oDex diffuses into the bulk gels/microgels, the local polymer density increases due to the additional hydrazone crosslinks. It was possible that the microgels stiffened with 0.1 wt% oDex were much stiffer than those stiffened with 0.05 wt% oDex, similar to that observed in bulk hydrogel stiffening (Fig. 2C). This is possible because based on the Flory–Rehner theory of rubber elasticity, the relationship between the hydrogel mesh size (and macroscopic sizes) and stiffness is not linear.[18] At sufficiently high polymer concentrations, a small increase in mesh size (which scales with the macroscopic hydrogel size) will result in a large increase in hydrogel elasticity. Nonetheless, through these experiments, we demonstrated that GelNB-CH, a dynamic macromer previously developed for mimicking the stiffening pancreatic tumor stroma, could be formulated into granular microgels. These microgels could be dynamically modified through a simple incubation step post-gelation (Fig. 2C). Although the current project mainly focused on dynamic stiffening, the carbohydrazide handles presented in the microgels could be leveraged for modular decoration of additional bioactive motifs, such as receptor ligands, fluorescent probes, drug molecules, or other macromolecules such as HA, as long as these molecules were modified with aldehyde groups. Additional orthogonal crosslinking or conjugation is also possible if the microgels were crosslinked with an excess norbornene group that can participate in a secondary thiol-norbornene photo-click reaction or tetrazine-norbornene iEDDA click reaction.

3.3. Culture of hMSCs on dynamically stiffened microgels

We aimed to demonstrate that GelNB-CH microgels could be leveraged for the 3D suspension culture of hMSCs. We first fabricated GelNB-CH bulk hydrogels and stiffened the hydrogels with 0.05 wt% oDex incubation. The storage moduli of the non-stiffened and oDex-stiffened bulk hydrogels (G'_{bulk}) were ~1.5 kPa and ~7.5 kPa, respectively. Next, GelNB-CH microgels (crosslinked by PEG4SH) were fabricated using the microfluidic droplet generator as described above, washed, and stiffened with 0.05 wt% oDex incubation overnight. Owing to the inherent cell adhesiveness of gelatin, hMSCs readily adhered and spread on the surface of both non-stiffened soft and oDex-stiffened GelNB-CH microgels (Fig. 4A). F-actin staining results showed that the seeded cells appeared to adhere more on the oDex-stiffened microgels, covering the entire microgel surface (Fig. 4A). On the other hand, cells on the non-stiffened microgels (*i.e.*, +0 wt% oDex, G' ~1.5 kPa) exhibited lower confluency. In addition to observing the cell morphology, we further stained collagen I and fibronectin deposited by the microgel-cultured hMSCs seven days after cell seeding on the microgels. We observed that cells adhered on both non-stiffened and oDex-stiffened microgels were able to secrete large quantities of these two ECM proteins (Fig. 4B), indicating that matrix protein synthesis was not impaired when cells were seeded on microgels with different stiffnesses.

Thiol-norbornene photopolymerization and hydrazone bonding are orthogonal reactions with demonstrated cytocompatibility for a variety of cell types.[19,20] Various 3D culture platforms have been developed for the culture, expansion, and differentiation of hMSCs *in vitro*, including encapsulation of hMSCs in engineered hydrogel scaffolds and aggregating hMSCs into multicellular spheroids.[21–23] Spheroid culture of hMSCs has many advantages, including extensive cell–cell interactions, generation of large cellular aggregates, and the flexible integration of bioreactors for stem cell expansion. However, matrix-free culture of hMSC spheroids does not provide a solid substrate that could mechanically stimulate the cells. In contrast, engineered hydrogels could provide tunable mechanics and matrix components to stimulate matrix mechanics-induced cell fate processes. However, one drawback of the conventional hydrogels was their nanometer-scale pores (or meshes) that would hinder rapid proliferation, limit nutrient transport, and reduce cell spreading.[24] In this regard, microcarriers/microgels are beneficial for 3D cell culture as they provide a higher surface-to-volume ratio for cell seeding and spreading than bulk gels.[25,26]

Furthermore, the use of microgels allows for the formation of cell-mediated microporous aggregates. Within these aggre-

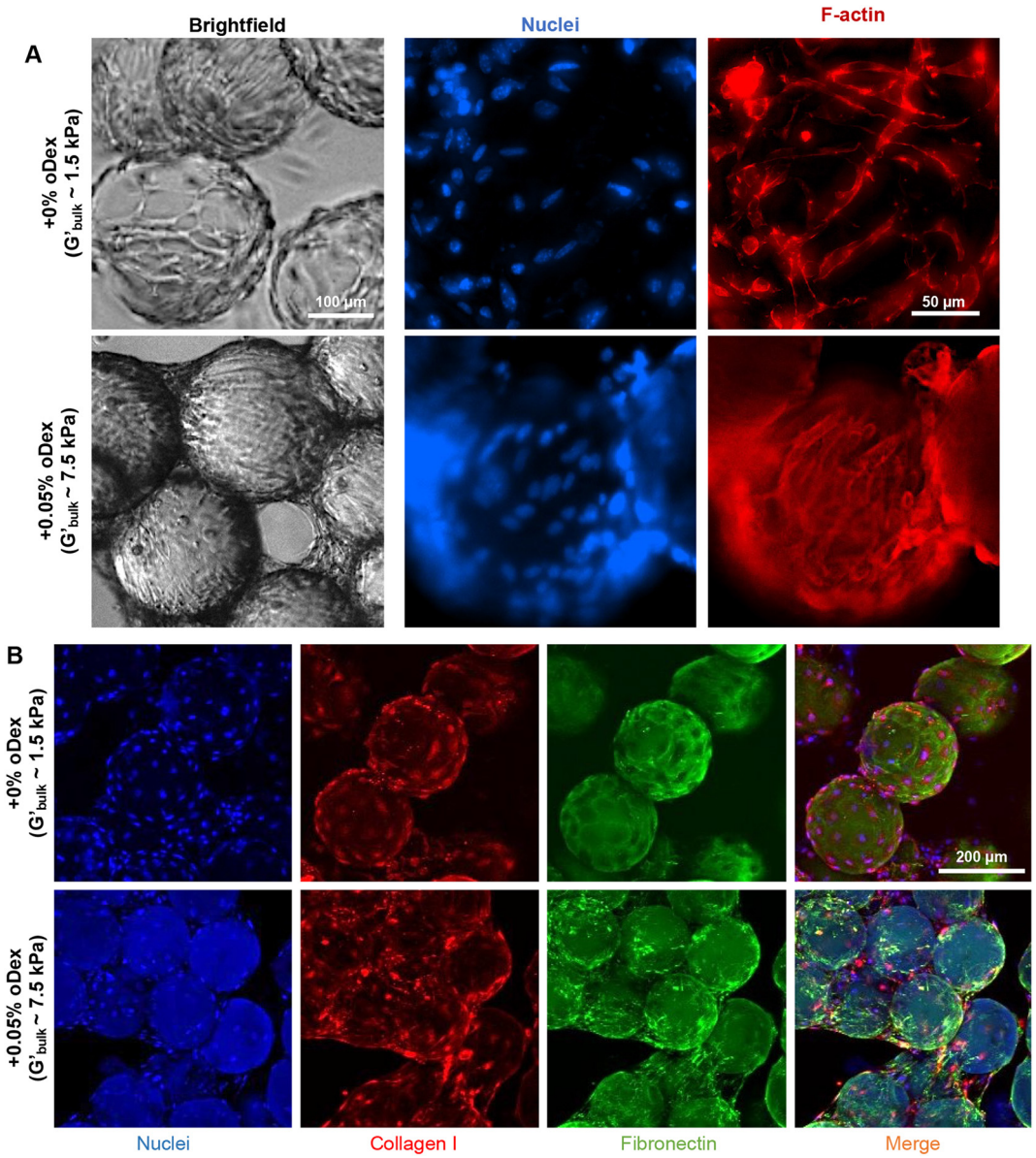

Fig. 4 GelNB-CH microgels as carriers for culturing hMSCs. (A) Phase contrast and nuclei/F-actin staining of hMSCs seeded on non-stiffened (+0 wt% oDex) and stiffened (+0.05 wt% oDex) GelNB-CH microgels. (B) Collagen I and fibronectin staining of hMSCs seeded on non-stiffened (+0 wt% oDex) and stiffened (+0.05 wt% oDex) GelNB-CH microgels.

gates, cells seeded on the microgels can spread freely in the same manner as cells cultured on a 2D surface, with the benefits of increasing cell–cell and cell–matrix interactions in all directions akin to 3D culture.[27]

Additionally, cell-laden microgels can be cultured in stirred bioreactors or spinner flasks for large-scale suspension culture, which has been shown to strongly increase hMSC proliferation, protein production, and the therapeutic efficacy.[28,29] Regardless of microgel stiffness, hMSCs secreted abundant ECM proteins collagen and fibronectin, which may strengthen their attachment to the microgel surface through increasing cell–matrix interactions.[30–34] Nonetheless, the dynamic culture of hMSCs on microgels with tunable properties has not been demonstrated. The current study established the feasibility of using GelNB-CH microgels for hMSC culture. Future work may focus on scaling up GelNB-CH microgel production for suspension cell culture.

3.4. Characterization of microgels fabricated through inverse suspension polymerization

Microgels can be mass produced by mechanically crushing/fragmenting a crosslinked bulk hydrogel[35,36] or by using inverse suspension polymerization.[15,37] While inverse suspension polymerization may produce microgels with a wider size distribution than those generated from microfluidic devices, the size variation can be significantly reduced by sieving the

polymerized microgels through a cell strainer with a defined size cut-off. Compared with mechanical fragmentation, the inverse suspension polymerization method yielded microgels with a smoother surface (*i.e.*, excluding the effect of roughness), which may be more desirable for interfacing with cells as the irregular shapes of the fragmented gels could potentially affect cell attachment and spreading. For example, it has been reported that the cell viability is lower when 3D-printed with fragmented microgels, as opposed to that with emulsion-derived spherical microgels.[38] Fragmented granular hydrogels also have a larger size distribution than those produced by either inverse suspension polymerization or microfluidic devices.[35]

To this end, we utilized an inverse suspension photopolymerization by mixing GelNB-CH, PEG4SH, and LAP in PBS and then emulsifying the mixture in the oil phase (Novec 7500) containing a surfactant. After thiol-norbornene photopolymerization, we excluded smaller microgels using 40 μm cell strainers and obtained microgels with a diameter range between 100 μm to 400 μm (Fig. 5A). Our preliminary studies (data not shown) showed that MAP gels can degrade within three days with the presence of cells. This phenomenon was likely due to a lower light penetration in the emulsion system and less homogeneous crosslinking due to variation of light exposure among the large number of micro-droplets. To increase the stability of the microgels fabricated through inverse suspension photopolymerization, we supplemented a synthetic polymer PEG8NB in the formulation. Microgels were successfully fabricated, and the thiol-to-norbornene ratio was estimated to be 0.47, which enabled further crosslinking during the annealing process. The stiffening was again achieved through oDex incubation, which led to a slight but significant decrease in microgel sizes (Fig. 5B). Specifically, the diameter of the microgels pre-stiffening was 168.8 ± 6.0 μm. After incubating with 0.01 wt%, 0.05 wt%, and 0.1 wt% oDex, the diameters changed to 179.8 ± 5.3 μm, 141.2 ± 3.7 μm, and 134.7 ± 4.6 μm (mean ± SEM), respectively. The microgel sizes post-oDex stiffening were similar to that obtained in microgels produced from microfluidic devices (Fig. 3B), but the size distributions were larger. This shrinkage dependence on oDex concentration was also observed for the averaged value of the 3 independent repeats (Fig. S3B†), where the size ranged from 181 ± 20.8 μm to 183.9 ± 3.4 μm, 167.8 ± 22.5 μm, and 153 ± 9.7 μm using 0.01, 0.05, and 0.1 wt% oDex for stiffening, respectively.

3.5. MAP gel fabrication through microgel annealing

The GelNB-CH-based microgels were crosslinked and stiffened by orthogonal thiol-norbornene and hydrazone click chemistry, respectively. These microgels may be further annealed through the third click chemistry – iEDDA click reaction between excess norbornene groups on GelNB-CH and an additional tetrazine-bearing macromer (*e.g.*, PEG4Tz, Fig. 6A). To effectively anneal all microgels into MAP gels, we re-dispersed the microgels homogeneously in PEG4Tz solution and packed the microgels through centrifugation. Using high molecular weight FITC-dextran, we assessed the void fractions of the MAP gels, which were between 20% and 40%, with higher void fractions in the TC-MAP gel assembled from microgels stiffened with higher oDex concentration (Fig. 6B and C). This was likely because the microgels were partially annealed during the oDex stiffening step, restricting the stiffened micro-

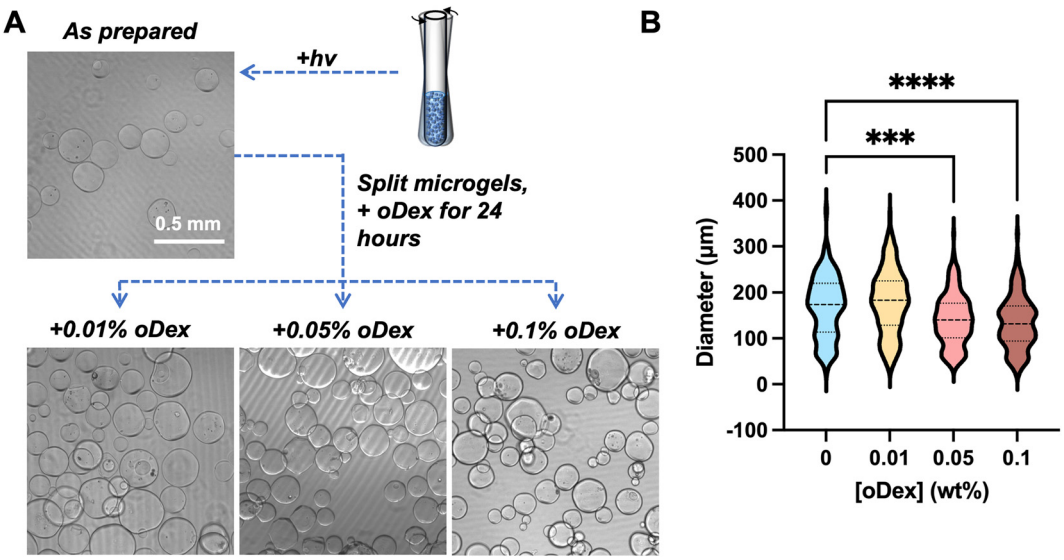

Fig. 5 Fabrication of GelNB-CH microgels *via* inverse suspension polymerization. (A) Representative images of non-stiffened (as prepared) GelNB-CH microgels and microgels stiffened with different oDex concentrations. Scale: 0.5 mm. (B) Quantification of diameters of non-stiffened and oDex-stiffened microgels fabricated by inverse suspension polymerization. 0 wt%: n = 123, 0.01 wt%: n = 172, 0.05 wt%: n = 230, and 0.1 wt%: n = 154. ***: $p < 0.001$ and ****: $p < 0.0001$. The statistical analyses in (B) are comparison between individual stiffened groups and control (0 wt% oDex).

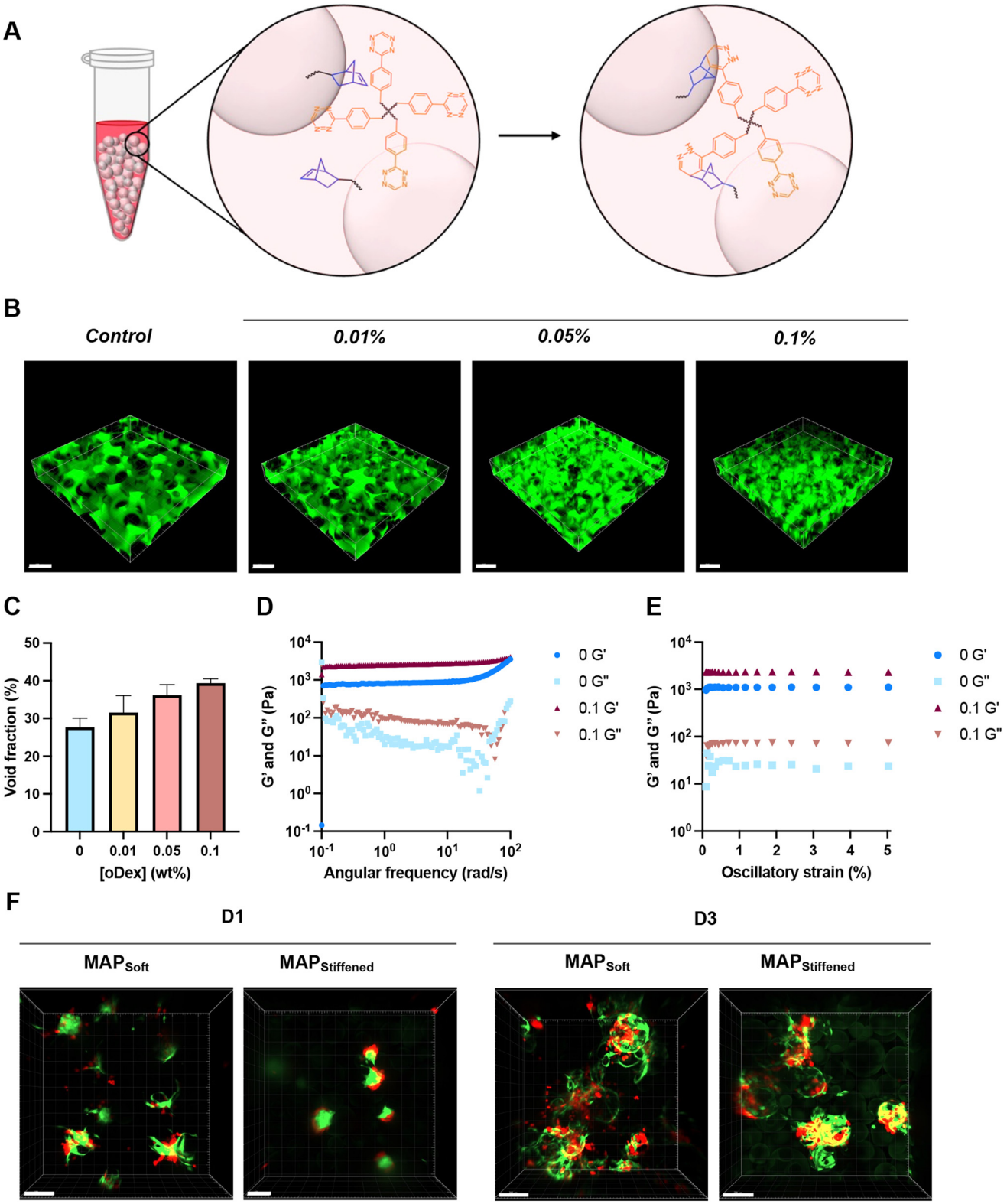

Fig. 6 Annealing of dynamically stiffened GelNB-CH microgels into TC-MAP scaffolds. (A) Microgels annealed *via* the iEDDA reaction between pendent norbornene and PEG4Tz. (B) MAP gels prepared with non-stiffened and oDex-stiffened GelNB-CH microgels perfused with FITC-dextran for visualization of the porous structure and (C) void fraction of the MAP gels. (D) Frequency sweep for non-stiffened (0 wt% oDex) and 0.1 wt% oDex-stiffened MAP gels. (E) Strain sweep for non-stiffened (0 wt% oDex) and 0.1 wt% oDex-stiffened MAP gels. (F) Pa03C + CAF spheroid encapsulated in MAP gel on D1 and D3. Data (n = 3 for all groups) presented in (C) are mean ± SEM, and there is no statistical difference between unstiffened and stiffened groups. Red and green in (F) represent Pa03C and CAF, respectively. Scale in (B) and (F): 200 μm.

gels from being further stacked during the annealing step. The stiffness of the MAP gels measured was tested within the linear viscoelastic range (Fig. 6D and E). The stiffness of the MAP gels remained unchanged over a week in PBS (Fig. S4†). Nevertheless, the stiffness of the stiffest TC-MAP gel was significantly higher than that of the non-stiffened MAP gel, suggesting that the stiffening on the single-microgel level could also alter the macroscopic stiffness of the MAP gel, despite having a higher void fraction. Since the MAP gels are porous and 20–40% of them were completely PBS, the stiffness difference among microgels stiffened with different concentrations of oDex could be even more significant than that shown in Fig. 6E and Fig. S4.† Also, the stiffness of the microgels would be more relevant to cells than that of the macroscopic MAP gels. Compared to the bulk gel stiffness shown in Fig. 2C, MAP gel stiffness was significantly lower. This is because both the void fraction and the gel fraction in MAP gel contributed to the overall stiffness, whereas bulk gel has no void fraction, whose stiffness was entirely derived from the gel fraction. Anderson *et al.* reported that the void fraction of MAP gel was also considered a bioactive cue for cell growth. They showed that mouse mesenchymal cells proliferated more in MAP gels with a higher void fraction, independent of the culture time.[39] The tetrazine-norbornene reaction has been used to anneal microgels.[4,8] The first step would always be microgel fabrication through the thiol-norbornene reaction, where norbornene is in excess. The second step is to utilize the remaining norbornene for the tetrazine-norbornene reaction as the binding mechanism for gel annealing. We adopted the same method, but since our stiffening is based on an orthogonal reaction, "stiffening capacity" of the stiffened gels remained the same as that of unstiffened ones. The void fractions of our MAP hydrogels were all higher than those fabricated by Anderson *et al.* (*i.e.*, 5%–17%) and comparable to others' results,[1,27,39] suggesting that the MAP gels would be permissive for cell growth.

3.6. *In vitro* cancer model using soft and stiff MAP gels

We have previously used GelNB-CH hydrogels as a dynamic culture platform to mimic the stiffening and increased deposition of HA in pancreatic ductal adenocarcinoma (PDAC).[7] Owing to the nanoscale meshes of the bulk hydrogels, however, significant spreading and proliferation of the encapsulated cancer cells were not notable within the first week. We reasoned that the highly porous TC-MAP hydrogels developed here would significantly reduce the time needed for cell spreading. To this end, we generated cancer cell spheroids from patient-derived Pa03C cells and cancer associated fibroblasts (CAF). The spheroids were then mixed with the GelNB-CH microgels prior to annealing into TC-MAP gels. As soon as one day post-encapsulation, notable spreading was observed from the mixed cell spheroids, especially in the softer TC-MAP gels (MAP_{soft}, Fig. 6F). By day 3, significant cell spreading was observed in both MAP_{soft} and MAP_{stiff} gels. Of note, CAF exhibited fibroblastic and migratory morphology and spread along the surface of multiple microgels, regardless of the MAP gel stiffness. On the other hand, cancer cells Pa03C spread into the void space between microgels in MAP_{soft} gels; but they were more aggregated and stayed close to each other in MAP_{stiff} gel. These results suggest that the physical properties of the microgels in MAP hydrogels played a role in their spreading even in the presence of CAFs, which are known to drive cancer cell migration through both direct cell–cell contact, ECM remodeling, and paracrine effects.[40–42]

Cells are known to respond to matrix stiffness through activating mechanosensors and organizing cytoskeletal structures, leading to altered gene expression, morphogenesis, and secretome.[30] Traditionally, cellular mechanosensing studies are conducted on 2D surfaces or in 3D matrices with a nanometer-scaled mesh size. However, when cells are encapsulated in mechanically stiff hydrogels, their movements are restricted by the dense matrix. Therefore, there is an unmet need to develop engineered matrices that provide mechanical stimulation to the cells without adversely affecting cellular morphogenesis in 3D. This is particularly important in the study of solid tumors (*e.g.*, PDAC and breast cancer), which have high stiffness due to desmoplastic reactions (*i.e.*, excessive accumulation of ECM, including collagen and HA).[43,44] During cancer cell dissemination *in vivo*, cells are known to travel from the stiffer tumor mass to the neighboring softer tissue, a phenomenon contradicting the finding of durotaxis on 2D substrates.[45] We are particularly interested in using the TC-MAP hydrogels described in this report to evaluate how cancer cells respond to 3D mechanical stimulation without the confounding factors of altered matrix crosslinking density. While microgels and MAP scaffolds have been widely used for biomedical application, only a few microgel studies focused on cancer-related research. Examples of microgels applied in cancer research include encapsulating cancer cells in microgels to study cancer spheroid formation with different microgel stiffness,[46] or using microgels as the anti-cancer agent.[47,48] To the best of our knowledge, no MAP hydrogel has been exploited for cancer research, and this study marks the first example of using dynamically tunable gelatin-based MAP gels for pancreatic cancer research.

4. Conclusion

Using GelNB-CH, an inherently bioactive and multi-responsive macromer, we have developed a new gelatin-based microgel system with dynamically tunable stiffness. Through triple-click chemistry, the GelNB-CH microgels can be fabricated *via* standard techniques, dynamically stiffened, and annealed into microporous hydrogels. We demonstrated that the dynamic GelNB-CH microgels can serve as 3D microcarriers for culturing hMSCs. We also fabricated TC-MAP hydrogels for studying the effect of matrix stiffness on cancer cell dissemination. In addition to the studies reported here, the GelNB-CH based TC-MAP system can be leveraged to study the effect of other matrix properties (*e.g.*, immobilization of biological molecules, such as HA) on cancer cell fate. Future work will also focus on

examining cancer cell dissemination across the interface of soft and stiff MAP gels, as well as isolating highly migratory cells for in-depth cellular and molecular analyses.

Conflicts of interest

There are no conflicts to declare.

Acknowledgements

This work was supported in part by the National Institutes of Health (R01CA227737, R01DK127436) and the Department of Defense (W81XWH2210864). The authors thank Dr Milessa Fishel for providing Pa03C cells and CAFs.

References

1 T. H. Qazi, V. G. Muir and J. A. Burdick, Methods to Characterize Granular Hydrogel Rheological Properties, Porosity, and Cell Invasion, *ACS Biomater. Sci. Eng.*, 2022, **8**(4), 1427–1442.
2 D. R. Griffin, W. M. Weaver, P. O. Scumpia, D. Di Carlo and T. Segura, Accelerated wound healing by injectable microporous gel scaffolds assembled from annealed building blocks, *Nat. Mater.*, 2015, **14**(7), 737–744.
3 Y. Liu, A. Suarez-Arnedo, L. Riley, T. Miley, J. Xia and T. Segura, Spatial Confinement Modulates Macrophage Response in Microporous Annealed Particle (MAP) Scaffolds, *Adv. Healthcare Mater.*, 2023, **12**(26), 2300823.
4 N. F. Truong, E. Kurt, N. Tahmizyan, S. C. Lesher-Pérez, M. Chen, N. J. Darling, W. Xi and T. Segura, Microporous annealed particle hydrogel stiffness, void space size, and adhesion properties impact cell proliferation, cell spreading, and gene transfer, *Acta Biomater.*, 2019, **94**, 160–172.
5 X. Zheng, Y. Hou, Q. Zhang, Y. Zheng, Z. Wu, X. Zhang and J.-M. Lin, 3D microgel with extensively adjustable stiffness and homogeneous microstructure for metastasis analysis of solid tumor, *Chin. Chem. Lett.*, 2023, **34**(11), 108319.
6 N. Zoratto, D. Di Lisa, J. de Rutte, M. N. Sakib, A. R. Alves e Silva, A. Tamayol, D. Di Carlo, A. Khademhosseini and A. Sheikhi, In situ forming microporous gelatin methacryloyl hydrogel scaffolds from thermostable microgels for tissue engineering, *Bioeng. Transl. Med.*, 2020, **5**(3), e10180.
7 C.-Y. Chang, H. C. Johnson, O. Babb, M. L. Fishel and C.-C. Lin, Biomimetic stiffening of cell-laden hydrogels via sequential thiol-ene and hydrazone click reactions, *Acta Biomater.*, 2021, **130**, 161–171.
8 A. Isaac, F. Jivan, S. Xin, J. Hardin, X. Luan, M. Pandya, T. G. H. Diekwisch and D. L. Alge, Microporous Bio-orthogonally Annealed Particle Hydrogels for Tissue Engineering and Regenerative Medicine, *ACS Biomater. Sci. Eng.*, 2019, **5**(12), 6395–6404.
9 Z. Mũnoz, H. Shih and C.-C. Lin, Gelatin hydrogels formed by orthogonal thiol–norbornene photochemistry for cell encapsulation, *Biomater. Sci.*, 2014, **2**(8), 1063–1072.
10 B. D. Fairbanks, M. P. Schwartz, A. E. Halevi, C. R. Nuttelman, C. N. Bowman and K. S. Anseth, A Versatile Synthetic Extracellular Matrix Mimic via Thiol-Norbornene Photopolymerization, *Adv. Mater.*, 2009, **21**(48), 5005–5010.
11 A. Jeanes and C. A. Wilham, Periodate Oxidation of Dextran, *J. Am. Chem. Soc.*, 1950, **72**(6), 2655–2657.
12 J. Maia, R. A. Carvalho, J. F. J. Coelho, P. N. Simões and M. H. Gil, Insight on the periodate oxidation of dextran and its structural vicissitudes, *Polymer*, 2011, **52**(2), 258–265.
13 Z. Jiang, F.-Y. Lin, K. Jiang, H. Nguyen, C.-Y. Chang and C.-C. Lin, Dissolvable microgel-templated macroporous hydrogels for controlled cell assembly, *Biomater. Adv.*, 2022, **134**, 112712.
14 A. S. Caldwell, V. V. Rao, A. C. Golden and K. S. Anseth, Porous bio-click microgel scaffolds control hMSC interactions and promote their secretory properties, *Biomaterials*, 2020, **232**, 119725.
15 A. S. Caldwell, G. T. Campbell, K. M. T. Shekiro and K. S. Anseth, Clickable Microgel Scaffolds as Platforms for 3D Cell Encapsulation, *Adv. Healthcare Mater.*, 2017, **6**(15), 1700254.
16 A. J. Rice, E. Cortes, D. Lachowski, B. C. H. Cheung, S. A. Karim, J. P. Morton and A. del Río Hernández, Matrix stiffness induces epithelial–mesenchymal transition and promotes chemoresistance in pancreatic cancer cells, *Oncogenesis*, 2017, **6**(7), e352–e352.
17 T. R. Cox and J. T. Erler, Remodeling and homeostasis of the extracellular matrix: implications for fibrotic diseases and cancer, *Dis. Models Mech.*, 2011, **4**(2), 165–178.
18 C.-C. Lin and K. S. Anseth, PEG Hydrogels for the Controlled Release of Biomolecules in Regenerative Medicine, *Pharm. Res.*, 2009, **26**(3), 631–643.
19 L. Koivusalo, J. Karvinen, E. Sorsa, I. Jönkkäri, J. Väliaho, P. Kallio, T. Ilmarinen, S. Miettinen, H. Skottman and M. Kellomäki, Hydrazone crosslinked hyaluronan-based hydrogels for therapeutic delivery of adipose stem cells to treat corneal defects, *Mater. Sci. Eng., C*, 2018, **85**, 68–78.
20 B. M. Richardson, D. G. Wilcox, M. A. Randolph and K. S. Anseth, Hydrazone covalent adaptable networks modulate extracellular matrix deposition for cartilage tissue engineering, *Acta Biomater.*, 2019, **83**, 71–82.
21 M. M. Hasani-Sadrabadi, P. Sarrion, S. Pouraghaei, Y. Chau, S. Ansari, S. Li, T. Aghaloo and A. Moshaverinia, An engineered cell-laden adhesive hydrogel promotes craniofacial bone tissue regeneration in rats, *Sci. Transl. Med.*, 2020, **12**(534), eaay6853.
22 L. Bian, C. Hou, E. Tous, R. Rai, R. L. Mauck and J. A. Burdick, The influence of hyaluronic acid hydrogel crosslinking density and macromolecular diffusivity on human MSC chondrogenesis and hypertrophy, *Biomaterials*, 2013, **34**(2), 413–421.

23 J. He, N. Zhang, Y. Zhu, R. Jin and F. Wu, MSC spheroids-loaded collagen hydrogels simultaneously promote neuronal differentiation and suppress inflammatory reaction through PI3K-Akt signaling pathway, *Biomaterials*, 2021, **265**, 120448.

24 S. R. Caliari, S. L. Vega, M. Kwon, E. M. Soulas and J. A. Burdick, Dimensionality and spreading influence MSC YAP/TAZ signaling in hydrogel environments, *Biomaterials*, 2016, **103**, 314–323.

25 C. Cha, J. Oh, K. Kim, Y. Qiu, M. Joh, S. R. Shin, X. Wang, G. Camci-Unal, K.-T. Wan, R. Liao and A. Khademhosseini, Microfluidics-Assisted Fabrication of Gelatin-Silica Core–Shell Microgels for Injectable Tissue Constructs, *Biomacromolecules*, 2014, **15**(1), 283–290.

26 W. Jiang, M. Li, Z. Chen and K. W. Leong, Cell-laden microfluidic microgels for tissue regeneration, *Lab Chip*, 2016, **16**(23), 4482–4506.

27 S. Xin, O. M. Wyman and D. L. Alge, Assembly of PEG Microgels into Porous Cell-Instructive 3D Scaffolds via Thiol-Ene Click Chemistry, *Adv. Healthcare Mater.*, 2018, **7**(11), 1800160.

28 F. Li, V. X. Truong, P. Fisch, C. Levinson, V. Glattauer, M. Zenobi-Wong, H. Thissen, J. S. Forsythe and J. E. Frith, Cartilage tissue formation through assembly of microgels containing mesenchymal stem cells, *Acta Biomater.*, 2018, **77**, 48–62.

29 J. M. Cha, E. K. Shin, J. H. Sung, G. J. Moon, E. H. Kim, Y. H. Cho, H. D. Park, H. Bae, J. Kim and O. Y. Bang, Efficient scalable production of therapeutic microvesicles derived from human mesenchymal stem cells, *Sci. Rep.*, 2018, **8**(1), 1171.

30 P. A. Janmey, D. A. Fletcher and C. A. Reinhart-King, Stiffness Sensing by Cells, *Physiol. Rev.*, 2020, **100**(2), 695–724.

31 F. Liu, D. Lagares, K. M. Choi, L. Stopfer, A. Marinković, V. Vrbanac, C. K. Probst, S. E. Hiemer, T. H. Sisson, J. C. Horowitz, I. O. Rosas, L. E. Fredenburgh, C. Feghali-Bostwick, X. Varelas, A. M. Tager and D. J. Tschumperlin, Mechanosignaling through YAP and TAZ drives fibroblast activation and fibrosis, *Am. J. Physiol.: Lung Cell. Mol. Physiol.*, 2015, **308**(4), L344–L357.

32 S. Noguchi, A. Saito, Y. Mikami, H. Urushiyama, M. Horie, H. Matsuzaki, H. Takeshima, K. Makita, N. Miyashita, A. Mitani, T. Jo, Y. Yamauchi, Y. Terasaki and T. Nagase, TAZ contributes to pulmonary fibrosis by activating profibrotic functions of lung fibroblasts, *Sci. Rep.*, 2017, **7**(1), 42595.

33 D. Kothapalli, S.-L. Liu, Y. H. Bae, J. Monslow, T. Xu, E. A. Hawthorne, F. J. Byfield, P. Castagnino, S. Rao, D. J. Rader, E. Puré, M. C. Phillips, S. Lund-Katz, P. A. Janmey and R. K. Assoian, Cardiovascular Protection by ApoE and ApoE-HDL Linked to Suppression of ECM Gene Expression and Arterial Stiffening, *Cell Rep.*, 2012, **2**(5), 1259–1271.

34 M. C. Prewitz, A. Stißel, J. Friedrichs, N. Träber, S. Vogler, M. Bornhäuser and C. Werner, Extracellular matrix deposition of bone marrow stroma enhanced by macromolecular crowding, *Biomaterials*, 2015, **73**, 60–69.

35 V. G. Muir, T. H. Qazi, J. Shan, J. Groll and J. A. Burdick, Influence of Microgel Fabrication Technique on Granular Hydrogel Properties, *ACS Biomater. Sci. Eng.*, 2021, **7**(9), 4269–4281.

36 A. M. Compaan, K. Song, W. Chai and Y. Huang, Cross-Linkable Microgel Composite Matrix Bath for Embedded Bioprinting of Perfusable Tissue Constructs and Sculpting of Solid Objects, *ACS Appl. Mater. Interfaces*, 2020, **12**(7), 7855–7868.

37 A. K. Fraser, C. S. Ki and C.-C. Lin, PEG-Based Microgels Formed by Visible-Light-Mediated Thiol-Ene Photo-Click Reactions, *Macromol. Chem. Phys.*, 2014, **215**(6), 507–515.

38 A. E. Widener, S. Duraivel, T. E. Angelini and E. A. Phelps, Injectable Microporous Annealed Particle Hydrogel Based on Guest–Host-Interlinked Polyethylene Glycol Maleimide Microgels, *Adv. NanoBiomed Res.*, 2022, **2**(10), 2200030.

39 A. R. Anderson, E. Nicklow and T. Segura, Particle fraction is a bioactive cue in granular scaffolds, *Acta Biomater.*, 2022, **150**, 111–127.

40 A. Labernadie, T. Kato, A. Brugués, X. Serra-Picamal, S. Derzsi, E. Arwert, A. Weston, V. González-Tarragó, A. Elosegui-Artola, L. Albertazzi, J. Alcaraz, P. Roca-Cusachs, E. Sahai and X. Trepat, A mechanically active heterotypic E-cadherin/N-cadherin adhesion enables fibroblasts to drive cancer cell invasion, *Nat. Cell Biol.*, 2017, **19**(3), 224–237.

41 E. Sahai, I. Astsaturov, E. Cukierman, D. G. DeNardo, M. Egeblad, R. M. Evans, D. Fearon, F. R. Greten, S. R. Hingorani, T. Hunter, R. O. Hynes, R. K. Jain, T. Janowitz, C. Jorgensen, A. C. Kimmelman, M. G. Kolonin, R. G. Maki, R. S. Powers, E. Puré, D. C. Ramirez, R. Scherz-Shouval, M. H. Sherman, S. Stewart, T. D. Tlsty, D. A. Tuveson, F. M. Watt, V. Weaver, A. T. Weeraratna and Z. Werb, A framework for advancing our understanding of cancer-associated fibroblasts, *Nat. Rev. Cancer*, 2020, **20**(3), 174–186.

42 B. Erdogan, M. Ao, L. M. White, A. L. Means, B. M. Brewer, L. Yang, M. K. Washington, C. Shi, O. E. Franco, A. M. Weaver, S. W. Hayward, D. Li and D. J. Webb, Cancer-associated fibroblasts promote directional cancer cell migration by aligning fibronectin, *J. Cell Biol.*, 2017, **216**(11), 3799–3816.

43 C. Tian, K. R. Clauser, D. Öhlund, S. Rickelt, Y. Huang, M. Gupta, D. R. Mani, S. A. Carr, D. A. Tuveson and R. O. Hynes, Proteomic analyses of ECM during pancreatic ductal adenocarcinoma progression reveal different contributions by tumor and stromal cells, *Proc. Natl. Acad. Sci. U. S. A.*, 2019, **116**(39), 19609–19618.

44 P. P. Provenzano, C. Cuevas, A. E. Chang, V. K. Goel, V. Hoff, D. Daniel and S. R. Hingorani, Enzymatic Targeting of the Stroma Ablates Physical Barriers to Treatment of Pancreatic Ductal Adenocarcinoma, *Cancer Cell*, 2012, **21**(3), 418–429.

45 C.-M. Lo, H.-B. Wang, M. Dembo and Y.-L. Wang, Cell Movement Is Guided by the Rigidity of the Substrate, *Biophys. J.*, 2000, **79**(1), 144–152.
46 H. Zhu, L. W. Y. Roode, A. J. Parry, N. A. Erkamp, M. Rodriguez-Garcia, M. Narita, Y. Shen, Y. Ou, Z. Toprakcioglu, M. Narita and T. P. J. Knowles, Core–Shell Spheroid-Laden Microgels Crosslinked under Biocompatible Conditions for Probing Cancer-Stromal Communication, *Adv. NanoBiomed Res.*, 2022, **2**(12), 2200138.
47 M. Majerská, M. Jakubec, V. Klimša, S. Rimpelová, V. Král and F. Štěpánek, Microgel Bioreactors for Cancer Cell Targeting by pH-Dependent Generation of Radicals, *Mol. Pharm.*, 2019, **16**(7), 3275–3283.
48 Q. Liu, Z. Yuan, X. Guo and J. H. van Esch, Dual-Functionalized Crescent Microgels for Selectively Capturing and Killing Cancer Cells, *Angew. Chem., Int. Ed.*, 2020, **59**(33), 14076–14080.